Supplementary Material (ESI) for Journal of Materials Chemistry A.
This journal is © The Royal Society of Chemistry 20xx

Electronic Supplementary Information (ESI)

Neighboring Effect Induced by V and Cr Doping in FeCoP Nanoarrays for Hydrogen Evolution Reaction with Pt-like Performance

Laifei Xiong,[a] Bin Wang,[a] Hairui Cai,[a] Tao Yang,[a]* Liqun Wang,[a] Shengchun Yang[a]*

a. School of Science, Key Laboratory of Shaanxi for Advanced Materials and Mesoscopic Physics, State Key Laboratory for Mechanical Behavior of Materials, Xi'an Jiaotong University, Xi'an, 710049, People's Republic of China

Corresponding Author

E-mail address: ysch1209@mail.xjtu.edu.cn (S. Y.); taoyang1@xjtu.edu.cn (T. Y.)

Experimental

Calculation of the active sites

The active sites of our samples were performed with a CHI 760E electrochemical workstation by using a typical three-electrode mode. The graphite rod and the Ag/AgCl (saturated KCl) electrode were used as counter electrode and reference electrode, and the samples (1 cm^2) were used as the working electrode. In brief, the electrochemical measurements were performed to obtain the consecutive cyclic voltammograms curves in 1 M PBS electrolyte (pH $\approx$ 7). The surface active site density is nearly in a linear relationship with the whole voltammetric charges (anodic and cathodic) over the CV curves. Thus, we assumed that oxidation and reduction are both one-electron process, and evaluated the upper limit number (n) of the active sites according to the following formula:

$$n = \frac{Q}{2F}$$

The Q and F correspond to the charge of the CV plot and Faraday constant, respectively. And the CV plots were tested from -0.2 to 0.6 V (vs RHE) with a scan rate of 50 mv s^{-1}.[1]

Calculation of The double-layer capacitances (C_{dl}) and electrochemical surface area (ECSA)

The double-layer capacitances (C_{dl}) of FeCoP and M-FeCoP were determined from their CV plots, which was used to evaluate the electrochemical surface areas (ECSA), and the CV plots were measured from -0.2 to -0.1 V (vs Ag/AgCl) with various scan rates (10, 20, 40, 60, 80, and 100 mV s^{-1}) in 0.5 M H_2SO_4. The ECSA was measured by cyclic voltammograms (CV) in the

non-Faradaic regions (where no charge-transfer reactions occur but absorption and desorption processes can take place). According to the equation: ECSA = $R_f \times S$, where the S and R_f are the geometric area and roughness of the electrode (here S = 1 cm^2), respectively. Based on the C_{dl} of a smooth oxide surface (60 μF cm^{-2}), the R_f is defined by Rf = C_{dl}/40 μF cm^{-2}.[2] Finally, the ECSA value is normalized with the current density by $j_{ECSA} = \frac{j}{ECSA}$.[3]

Calculation of turnover frequency (TOF)

We assumed that all the active sites were in full contact with the electrolyte, and the TOF values (s^{-1}) were calculated with the equation as follows:

$$TOF = \frac{I}{2Fn}$$

Where these physical variables represent as follows:

I represent the current (A) during hydrogen evolution in 0.5 M H_2SO_4.

F represent the Faraday constant (~ 96485 C/mol).

n represent the number of active sites (mol).

1/2 represent two electrons and protons are existed to evolve a hydrogen molecule (H_2) during the HER process, so the factor is 1/2.

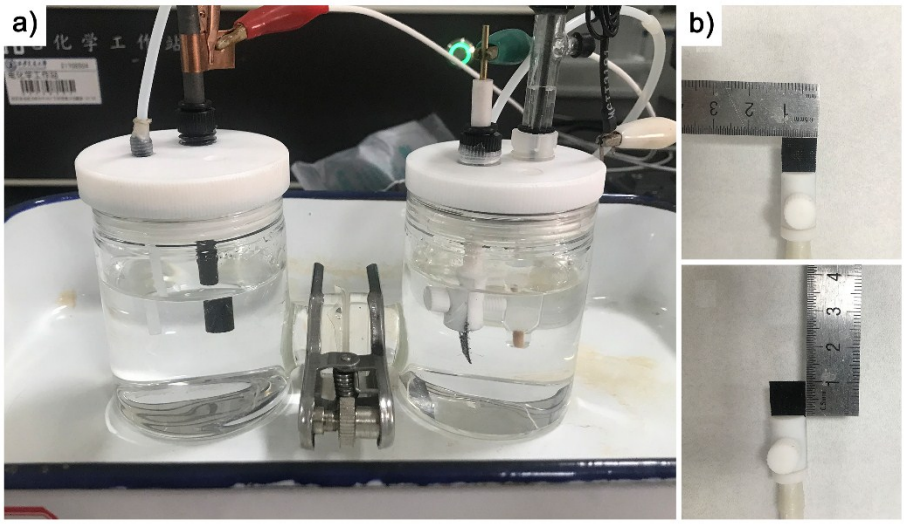

Fig. S1. a) The H-type electrolytic cell. b) 1 cm × 1 cm size of the sample.

The H-type electrolytic cell was used for the electrochemical measurements, and the ion-exchange membrane was applied to separate the working electrode from the counter electrode.

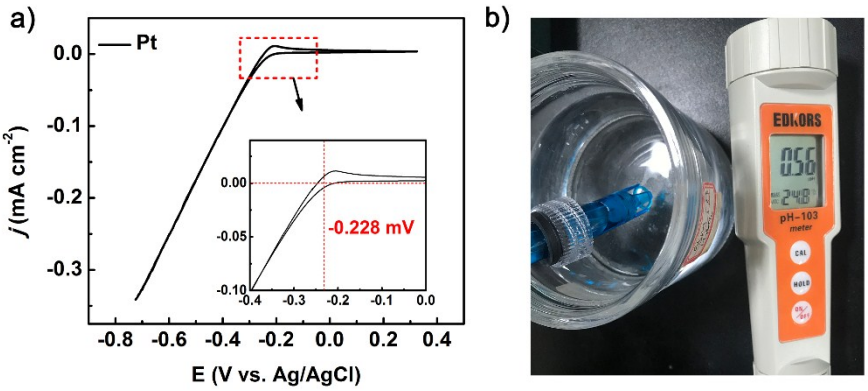

Fig. S2. a) The calibration CV curve of Ag/AgCl reference electrode. b) The pH value of the acid solution.

All the potentials measured in this work were converted into a commonly used reversible hydrogen electrode (RHE). The conversion Nernst equation are *E* (V *vs.* RHE) = *E* (V *vs.* Ag/AgCl) + 0.0591 × pH + 0.198 for the Ag/AgCl reference electrodes, respectively. Moreover, the reference electrode was calibrated by cyclic voltammetry (CV) under the acid solution (saturated H_2), and the calibration result was consistent with the value (RHE) converted by the Nernst equation.

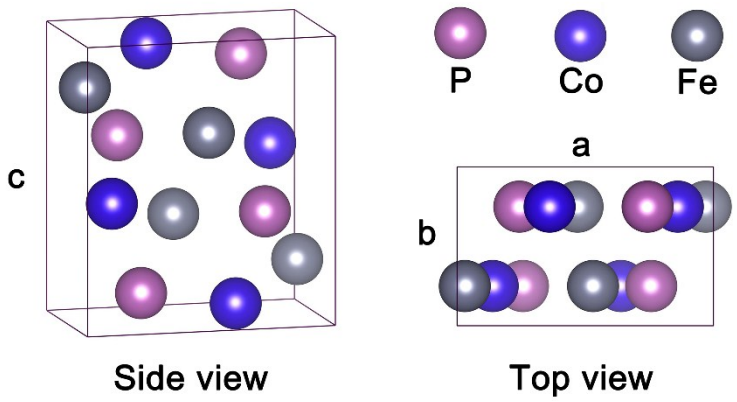

Fig. S3. Side and top views of the optimized structure of FeCoP.

The initial lattice parameters of model catalyst is a = 5.71, b = 3.53, and c = 6.53 Å, The optimized lattice parameters is a = 5.43, b = 3.54, and c = 6.61 Å.

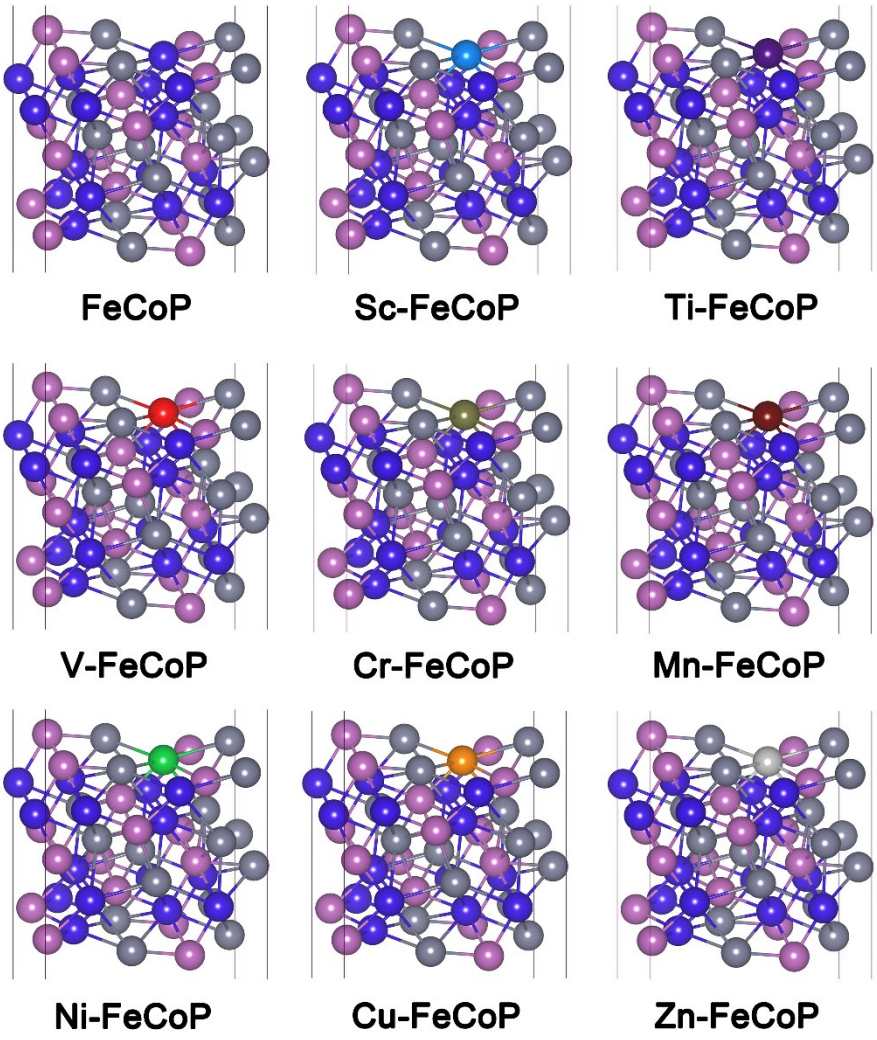

Fig. S4. Side views of the optimized structure of M-FeCoP (M = Sc, Ti, V, Cr, Mn, Ni, Cu, and Zn).

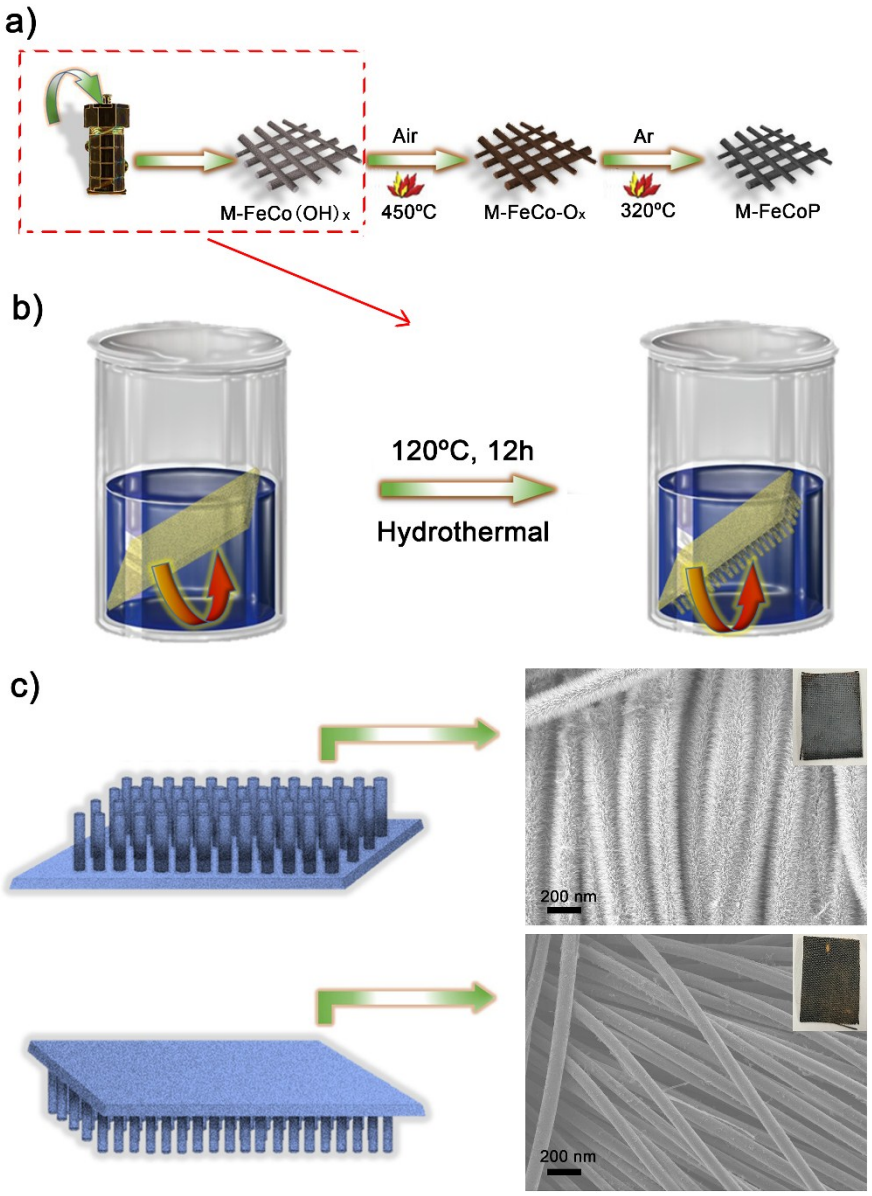

Fig. S5. a) Schematic illustration of the synthesis process for M-FeCoP. b) Schematic illustration of synthesis process for M-FeCo(OH)$_x$. c) The illustration and SEM images of lower and upper surface of carbon cloth, respectively. The inset in c) are the corresponding optical picture. It is clear that M-FeCo(OH)$_x$ nanoarrays were grown at the lower surface of carbon cloth after the hydrothermal reaction (M = Zn, V, Ni, Cr, and Mn).

In brief, the M-FeCo$(OH)_x$ precursor nano-rod arrays were firstly grown on the lower surface of CC by a hydrothermal method, followed by sintering in air to increase the crystallinity and durability of the materials. Then, the materials were phosphatized by using NaH_2PO_2 as phosphorus source to obtain M-FeCoP.

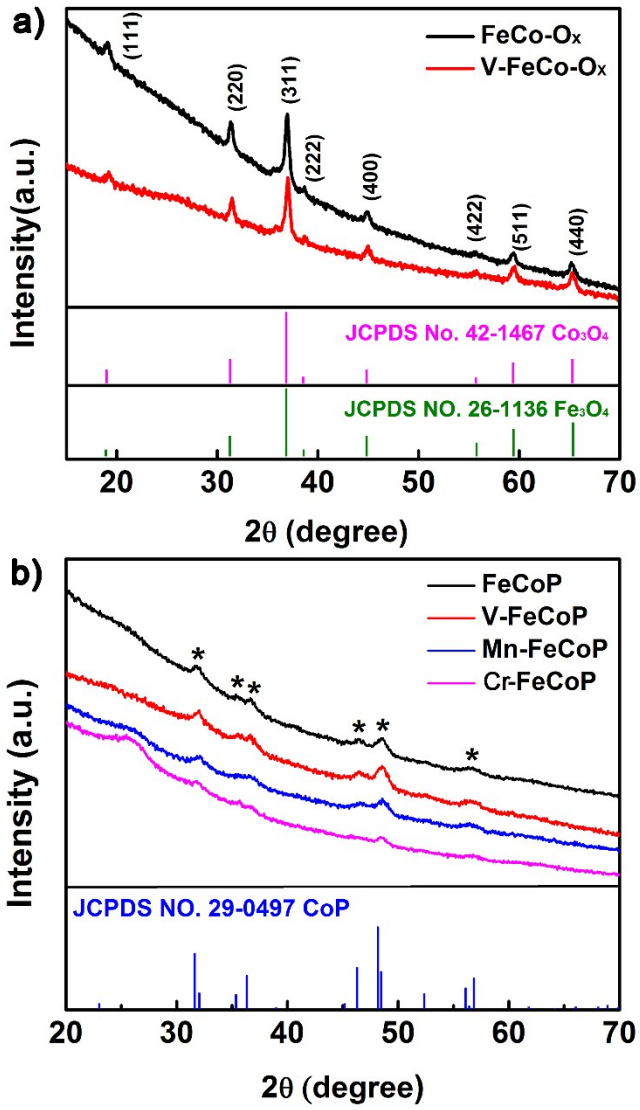

Fig. S6. a) XRD patterns of FeCo-O_x and V-FeCo-O_x. b) XRD patterns of FeCoP and M-FeCoP (M = V, Mn, and Cr).

X-ray diffraction (XRD) patterns (Fig. S6) reveal the spinel structure of Co_3O_4 (PDF # 42-1467) and Fe_3O_4 (PDF # 26-1136) for the FeCo-O_x and V-FeCo-O_x precursor. After phosphorization, both samples of FeCoP and M-FeCoP supported on CC are found to be well matched to the orthorhombic phase of CoP (PDF # 29-0497).

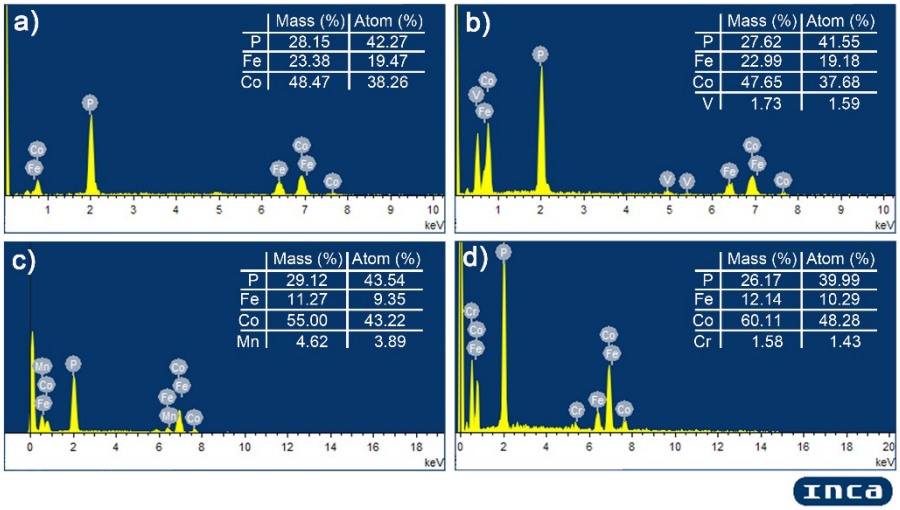

Fig. S7. The EDX spectrum of a) FeCoP, b) V-FeCoP, c) Mn-FeCoP, and d) Cr-FeCoP, respectively. The feeding amount of samples are $Co(NO_3)_2 \cdot 6H_2O$ = 0.6 mmol, $Fe(NO_3)_3 \cdot 9H_2O$ = 0.6 mmol.

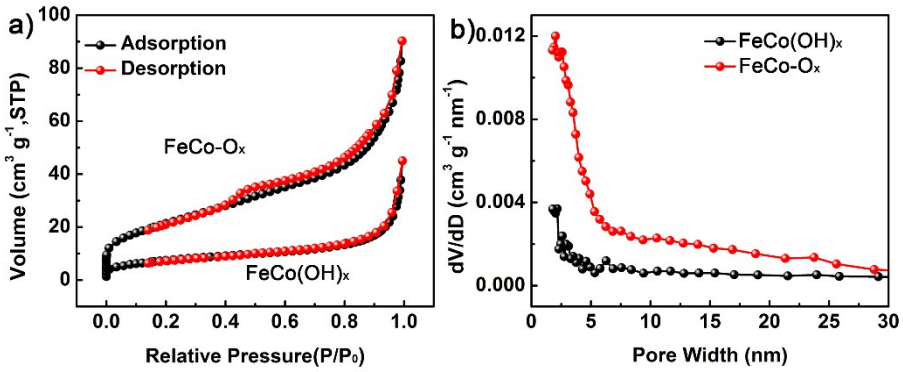

Fig. S8. a) The N_2 adsorption/desorption isotherms of $FeCo(OH)_x$ and $FeCo\text{-}O_x$. b) Pore size distributions of $FeCo(OH)_x$ and $FeCo\text{-}O_x$.

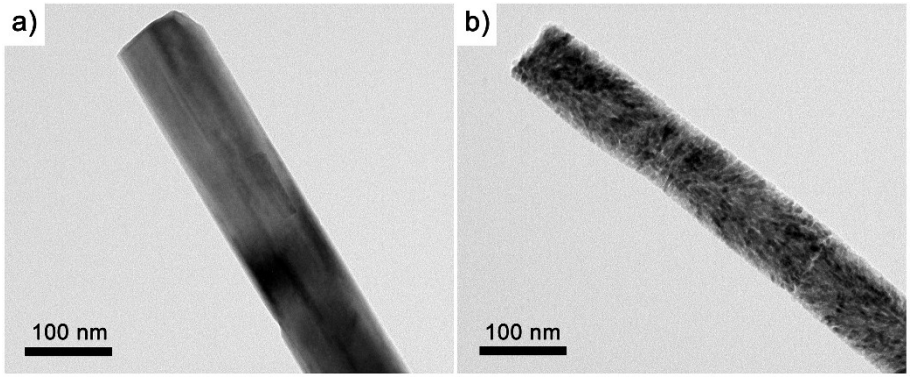

Fig. S9. a) The TEM image of the $FeCo(OH)_x$ precursor. b) The TEM image of the $FeCo\text{-}O_x$ precursor after sintering.

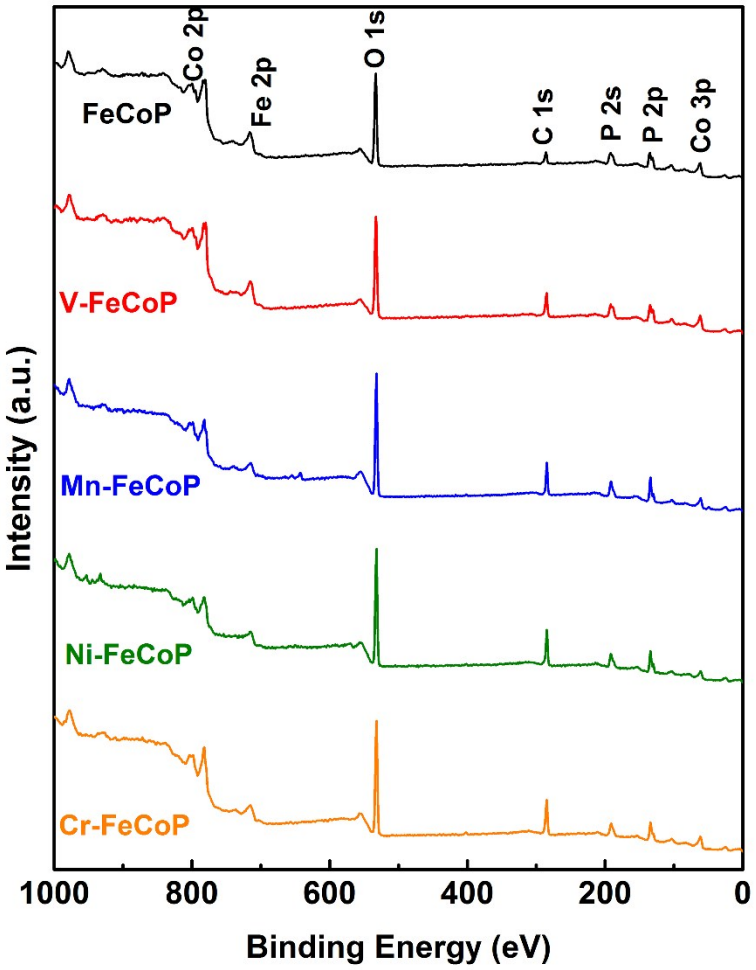

Fig. S10. XPS survey spectra of FeCoP and M-FeCoP (M = V, Mn, Ni, and Cr).

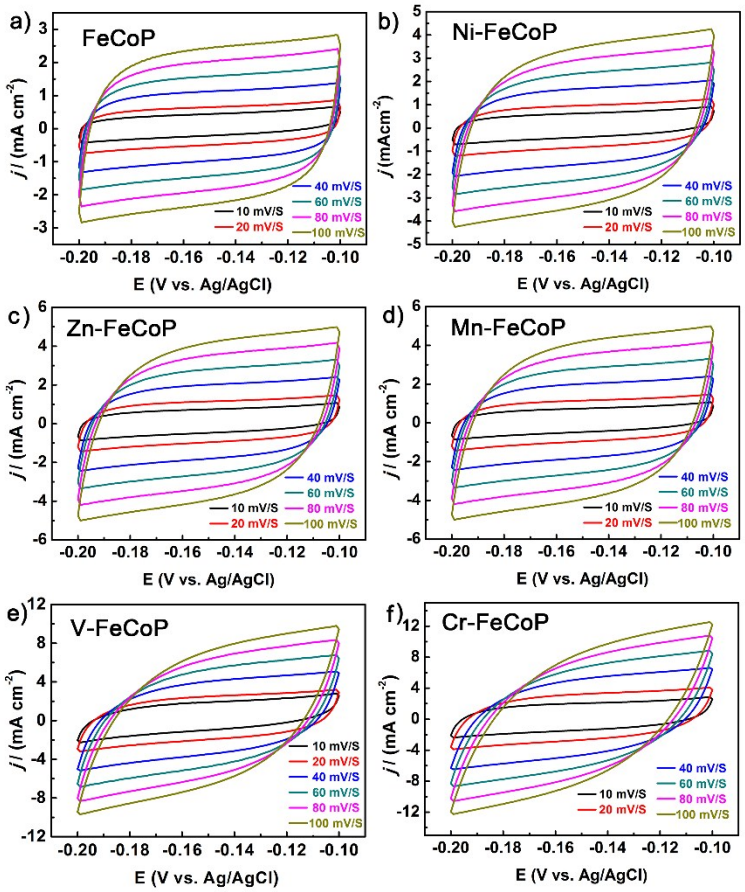

Fig. S11. CVs performed at various scan rates in the region of -0.2 V to -0.1 V (vs. Ag/AgCl) for a) FeCoP, b) Ni-FeCoP, c) Zn-FeCoP, d) Mn-FeCoP, e) V-FeCoP, and f) Cr-FeCoP.

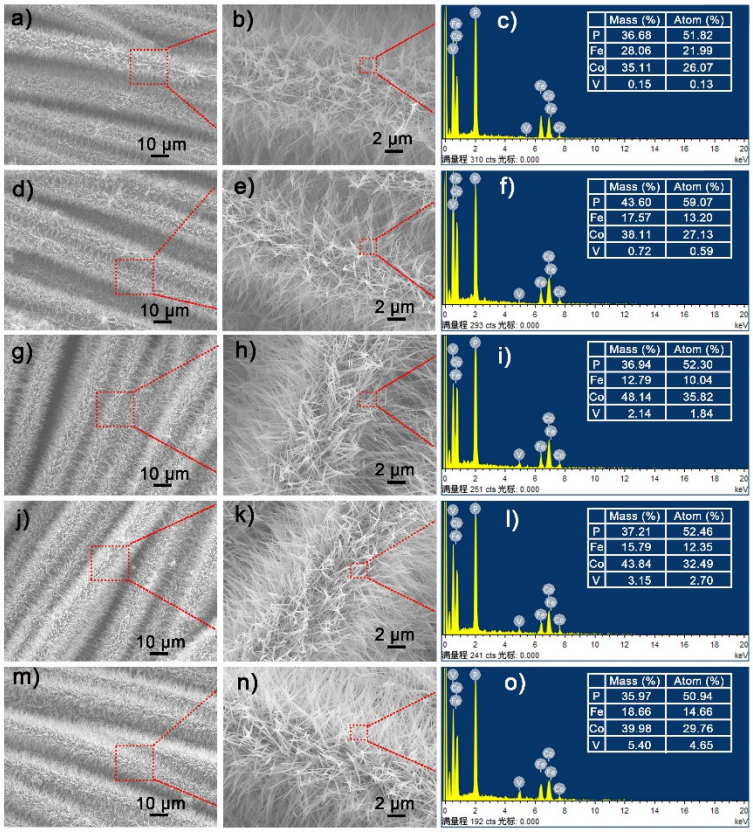

Fig. S12. The corresponding SEM images and EDX spectra and element ratios for a) – c) V-FeCoP-1, d) – f) V-FeCoP-5, g) – i) V-FeCoP-10, j) – l) V-FeCoP-15, and m) – o) V-FeCoP-20. The feeding amount of samples are $Co(NO_3)_2 \cdot 6H_2O$ = 0.6 mmol, $Fe(NO_3)_3 \cdot 9H_2O$ = 0.6 mmol, VCl_3 = 1 , 5, 10, 15, and 20 (mg).

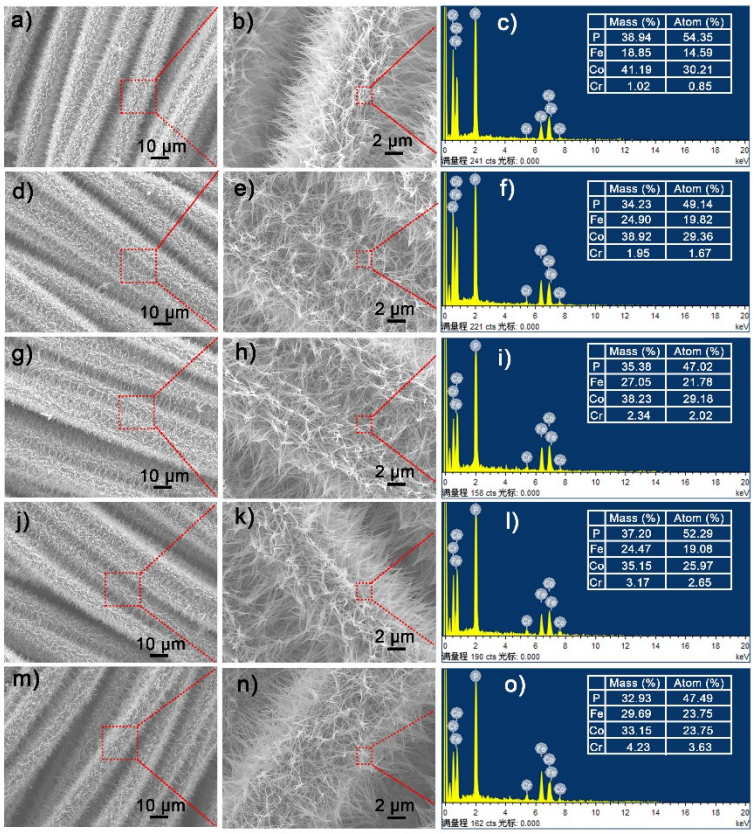

Fig. S13. The corresponding SEM images and EDX spectra and element ratios for a) – c) Cr-FeCoP-5, d) – f) Cr-FeCoP-10, g) – i) Cr-FeCoP-15, j) – l) Cr-FeCoP-20, and m) – o) Cr-FeCoP-25. The feeding amount of samples are $Co(NO_3)_2 \cdot 6H_2O$ = 0.6 mmol, $Fe(NO_3)_3 \cdot 9H_2O$ = 0.6 mmol, $CrCl_3$ = 5, 10, 15, 20, and 25 (mg).

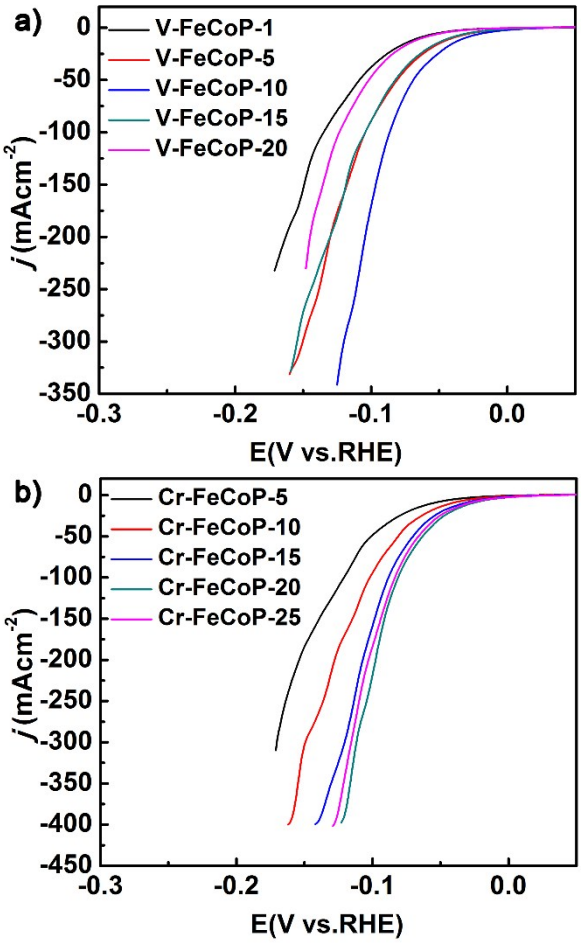

Fig. S14. Polarization curves of M-FeCoP samples with different M doping amount for a) V-FeCoP and b) Cr-FeCoP (M-FeCoP-x, the x (mg) represent the feeding amount of heteroatoms).

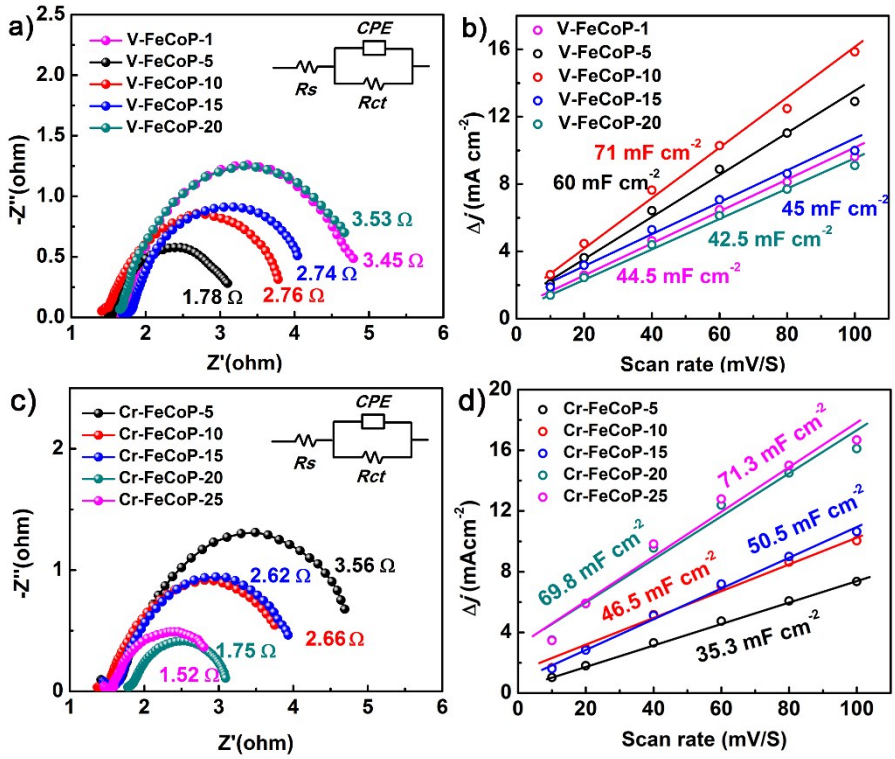

Fig. S15. a) Nyquist plots of V-FeCoP-x with different V amount. b) Capacitive currents as a function of scan rate for V-FeCoP-x with different V amount. c) Nyquist plots of Cr-FeCoP-x with different Cr amount. d) Capacitive currents as a function of scan rate for Cr-FeCoP-x with different Cr amount.

The electrochemical impedance spectroscopy (EIS) for the FeCoP catalyst with the different heteroatoms (V and Cr) feeding amount were also tested. The charge transfer resistance (R_{ct}) as shown in Fig. S13a, the R_{ct} values of V-FeCoP-x catalysts (x = 1, 5, 10, 15, and 20) are 3.45, 1.78, 2.76, 2.74, and 3.53 Ω, respectively. In Fig. S13b the electrochemical double-layer capacitance (C_{dl}) were recorded, and the C_{dl} values of V-FeCoP-x catalysts (x = 1, 5, 10, 15, and 20) are 44.5, 60, 71, 45, and 42.5 mF cm^{-2}, respectively, that has the same tendency as the LSV curves. In Fig. S 13c, he R_{ct} values of Cr-FeCoP-x catalysts (x = 5, 10, 15, 20, and 25) are 3.56,

2.66, 2.62, 1.75, and 1.52 Ω, respectively. In Fig. S13d, the C_{dl} values of Cr-FeCoP-x catalysts (x = 5, 10, 15, 20, and 25) are 35.3, 46.5, 50.5, 69.8, and 71.3 mF cm^{-2}, respectively.

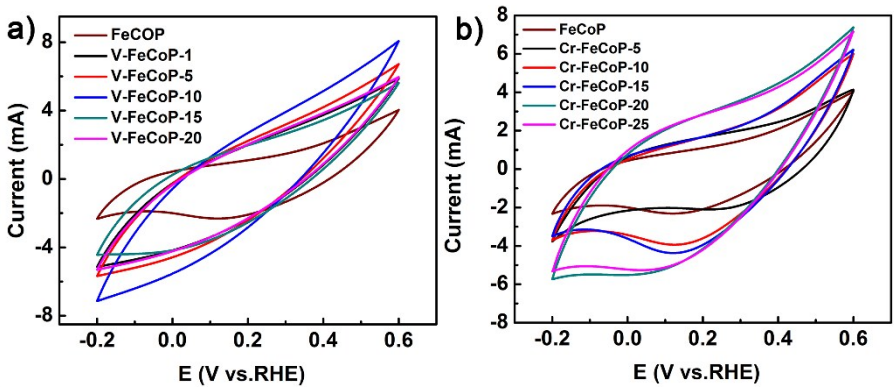

Fig. S16. a) CVs performed at 50 mV S^{-1} scan rates in the region of -0.2 V to -0.6 V (vs RHE) in PBS solution for FeCoP and V-FeCoP-x. b) CVs performed at 50 mV S^{-1} scan rates in the region of -0.2 V to -0.6 V (vs RHE) in PBS solution for FeCoP and Cr-FeCoP-x.

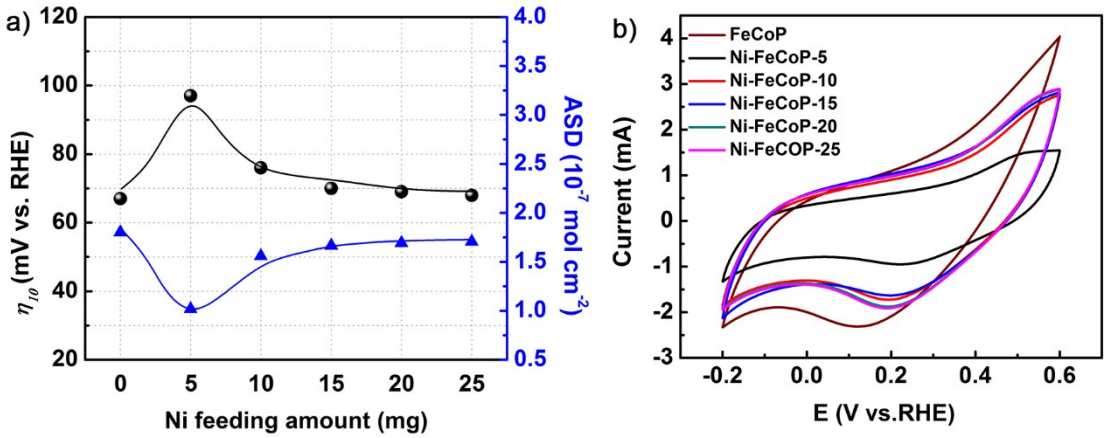

Fig. S17. a) The corresponding overpotentials at the current density of 10 mV cm^{-2} and the active site density (ASD) with different Ni doping amount. b) CVs performed at 50 mV S^{-1} scan rates in the region of -0.2 V to -0.6 V (vs RHE) in PBS solution for FeCoP and Ni-FeCoP-x.

In Fig. S17, the values of η_{10} present a maximum when feeding amount of Ni is 5 mg, and further increasing Ni doping amount obviously decreases such value in HER, which is in consistence with the change tendency of ASD.

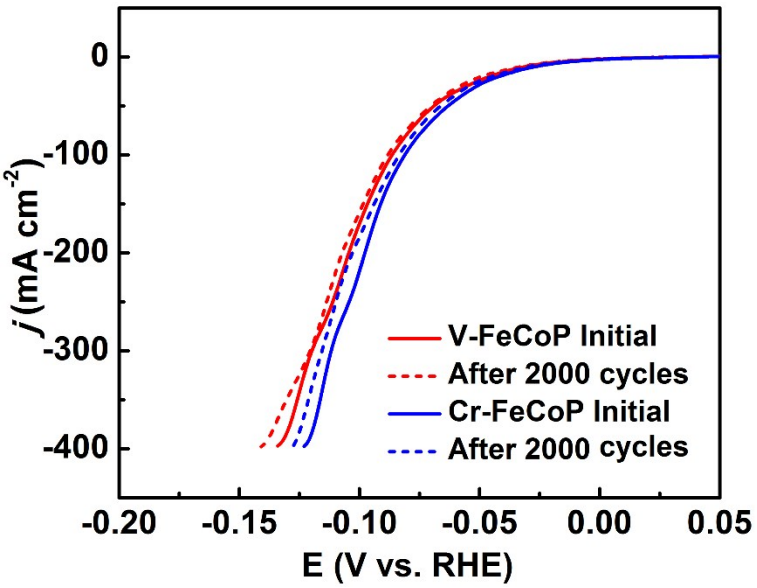

Fig. S18. Polarization curves of V-FeCoP and Cr-FeCoP initial and after 2000 CV cycles.

Table S1. The charge transfer amount from M to Fe, Co and P atoms. (M = Sc, Ti, V, Cr, Mn, and Zn).

Heteroatoms(M)	Bader charge (e)	Host atoms	Amount of charge transfer (e)
Sc	1.17	Fe	-0.17
		Co	-0.10
		P	-0.17
Ti	1.04	Fe	-0.16
		Co	-0.06
		P	-0.16
V	0.78	Fe	-0.11
		Co	-0.04
		P	-0.12
Cr	0.53	Fe	-0.07
		Co	-0.03
		P	-0.09
Mn	0.37	Fe	-0.05
		Co	-0.02
		P	-0.06
Zn	0.24	Fe	-0.02
		Co	-0.03
		P	-0.05

Compared with the electronic structure of FeCoP, the Bader charge of Fe, Co and P is 0.51, 0.03, and -0.53 e. Thus, the charge of Sc (1.17 e) transfer to Fe (-0.17 e), Co (-0.10 e), and P (-0.17 e) in Sc-FeCoP; the charge of Ti (1.04 e) transfer to Fe (-0.16 e), Co (-0.06 e), and P (-0.16

e) in Ti-FeCoP; the charge of V (0.78 e) transfer to Fe (-0.11 e), Co (-0.04 e), and P (-0.12 e) in V-FeCoP; the charge of Cr (0.53 e) transfer to Fe (-0.07 e), Co (-0.03 e), and P (-0.09 e) in Cr-FeCoP; the charge of Mn (0.37 e) transfer to Fe (-0.05 e), Co (-0.02 e), and P (-0.06 e) in Mn-FeCoP; the charge of Zn (0.24 e) transfer to Fe (-0.02 e), Co (-0.03 e), and P (-0.05 e) in Zn-FeCoP.

Table S2. The ΔG_{H^*} of different active sites on FeCoP and M-FeCoP (M = Sc, Ti, V, Cr, Mn, Ni, Cu, and Zn).

Compound	Structure	Active sites	ΔG_{H^*} (eV)
FeCoP	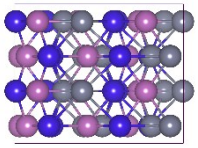	Co	-0.24
		Fe	-0.31
Sc-FeCoP	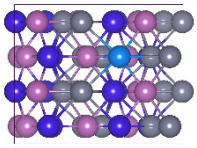	Co	-0.46
		Fe	-0.43
		Sc	-0.43
Ti-FeCoP	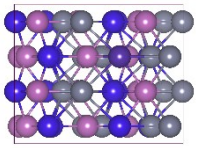	Co	-0.37
		Fe	-0.44
		Ti	-0.44
V-FeCoP	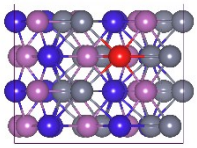	Co	-0.15
		Fe	-0.38
		V	-0.43
Cr-FeCoP	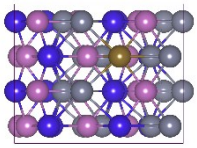	Co	-0.1
		Fe	-0.31
		Cr	-0.31
Mn-FeCoP	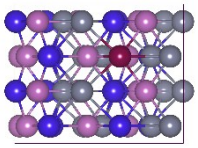	Co	-0.19
		Fe	-0.37
		Mn	-0.37
Ni-FeCoP	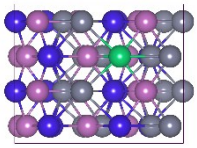	Co	-0.22
		Fe	-0.27
		Ni	-0.04
Cu-FeCoP	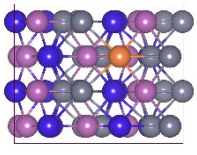	Co	-0.26

		Fe	-0.07
		Cu	0.05
Zn-FeCoP	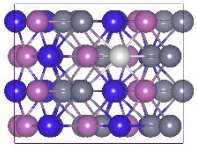	Co	-0.29
		Fe	-0.25
		Zn	0.3

Table. S3 The BET Surface Area and average pore with of FeCo-O_x and FeCo$(OH)_x$.

Catalyst-precursor	BET Surface Area (m^2 g^{-1})	Average pore width (nm)
FeCo-O_x	77.3798	7.223
FeCo$(OH)_x$	26.5461	10.495

Table S4. The ΔG_{H^*} of different active sites on FeCoP and V-FeCoP.

Compound	Site	ΔG_{H^*} (eV)
FeCoP	Fe	-0.31
	Co	-0.24
	P	0.38
V-FeCoP	Fe	-0.38
	Co	-0.15
	P	0.43
	V	-0.43

Table. S5 Comparison of V-FeCoP with other non-noble metal-based catalysts in terms of HER performance in acidic medium.

Catalyst	*η10* (mV)	Tafel Slope (mV dec^{-1})	Stability	Ref.
V-FeCoP	**32**	**47**	**2000 CV/90 h**	**This work**
Cr-FeCoP	**28**	**45**		
$Fe_{0.5}Co_{0.5}P$/CC	37	37	3000 CV/100 h	4
CC@N-CoP	42	41.2	5000 CV/20 h	5
Cu-CoP NRAs/CC	44	102	40 h	6
V-CoP/CC	47	67.6	3000 CV/25 h	7
NiCu@C-1	48	63.2	2000 CV/10 h	8
FeP/Fe@NC	49	67	5000 CV/90 h	9
Fe_3P	49	57	20 h	10
Ce-doped CoP	54	54	10 h	11
HP-$NiSe_2$	57	43	1000 CV/1 h	12
MoP_2 NS/CC	58	63.6	2000 CV/20 h	13
FeP_2	61	37	8 h	14
Ni_2P-NPCNFs-CC	63.2	56.7	3000 CV/33 h	15
FeCo@FeCoP@C	65	60	1000 CV/10 h	16
FeP film	65	48.5	5000 CV/18 h	17
FeP SS	66	45	24 h	18
FeP/C with shell	71	52	10000 CV/44 h	19
CoP@PS/NCNT	80	53	1000 CV/4 h	20
CoP/PCNF-0.4	83	62	3000 CV/11 h	21
ReSSe NDs	84	50.1	20000 CV	22
CF@NPC-MoP	87	49.1	2000 CV/20 h	23

Cu_3P@NPPC-650	89	76	3000 CV/12 h	24
SWCNTs/$MoSe_2$	100	63	-	25
CoP/rGO-400	105	50	3000 CV/22 h	26
MS-QDs	108	53	16000 CV	27
FeP/NCNSs	114	64	5000 CV/20 h	28
HMFeP@C	115	56	3000 CV/22 h	29
CoP3/Ni2P	115	49	10000 CV/40 h	30
CoP@C-NPs/GA-5	120	57	1000 CV/3.3 h	31
CoP/CFP-H	128.1	49.7	2000 CV/24 h	32
$Mo_{0.37}W_{0.63}S_2$/C	137	53	3000 CV/3 h	33
CoP-CNTs	139	52	2000 CV/20 h	34
$Fe_{4.5}Ni_{4.5}S_8$	146	-	20 h	35
α-MoB_2	149	-	15000 CV/30 h	36
CoP/WSe_2-4	163	76.5	1000 CV/21 h	37
TpPAM	250	106	1000 CV/5 h	38

η_{10}: Overpotential of the catalysts at a current density of 10 mA cm^{-2}.

CC: carbon cloth

References

1 D. Merki, S. Fierro, H. Vrubel and X. Hu, *Chem. Sci.*, 2011, **2**, 1262-1267.
2 R. Zhang, X. Ren, S. Hao, R. Ge, Z. Liu, A. M. Asiri, L. Chen, Q. Zhang and X. Sun, *J. Mater. Chem. A*, 2018, **6**, 1985-1990.
3 D. Voiry, M. Chhowalla, Y. Gogotsi, N. A. Kotov, Y. Li, R. M. Penner, R. E. Schaak and P. S. Weiss, *ACS Nano*, 2018, **12**, 9635-9638.
4 C. Tang, L. Gan, R. Zhang, W. Lu, X. Jiang, A. M. Asiri, X. Sun, J. Wang and L. Chen, *Nano Lett.*, 2016, **16**, 6617-6621.
5 Q. Zhou, Z. Shen, C. Zhu, J. Li, Z. Ding, P. Wang, F. Pan, Z. Zhang, H. Ma, S. Wang and H. Zhang, *Adv. Mater.*, 2018, **30**, 1800140.
6 L. Wen, Y. Sun, C. Zhang, J. Yu, X. Li, X. Lyu, W. Cai and Y. Li, *ACS Appl. Energy Mater.*, 2018, **1**, 3835-3842.
7 X. Xiao, L. Tao, M. Li, X. Lv, D. Huang, X. Jiang, H. Pan, M. Wang and Y. Shen, *Chem. Sci.*, 2018, **9**, 1970-1975.
8 Y. Shen, Y. Zhou, D. Wang, X. Wu, J. Li and J. Xi, *Adv. Energy Mater.*, 2018, **8**, 1701759.
9 X. Wang, W. Ma, Z. Xu, H. Wang, W. Fan, X. Zong and C. Li, *Nano Energy*, 2018, **48**, 500-509.
10 D. E. Schipper, Z. Zhao, H. Thirumalai, A. P. Leitner, S. L. Donaldson, A. Kumar, F. Qin, Z. Wang, L. C. Grabow, J. Bao and K. H. Whitmire, *Chem. Mater.*, 2018, **30**, 3588-3598.
11 W. Gao, M. Yan, H.-Y. Cheung, Z. Xia, X. Zhou, Y. Qin, C.-Y. Wong, J. C. Ho, C.-R. Chang and Y. Qu, *Nano Energy*, 2017, **38**, 290-296.
12 H. Zhou, F. Yu, Y. Liu, J. Sun, Z. Zhu, R. He, J. Bao, W. A. Goddard, S. Chen and Z. Ren, *Energy Environ. Sci.*, 2017, **10,** 1487-1492..
13 W. Zhu, C. Tang, D. Liu, J. Wang, A. M. Asiri and X. Sun, *J. Mater. Chem. A*, 2016, **4**, 7169-7173.
14 C. Y. Son, I. H. Kwak, Y. R. Lim and J. Park, *Chem. Commun.*, 2016, **52**, 2819-2822.
15 M.-Q. Wang, C. Ye, H. Liu, M. Xu and S.-J. Bao, *Angew. Chem. Int. Ed.*, 2018, **15**, 1963-1967.
16 J. Zhang, M. Li, X. Liang and Z. Zhuang, *ACS Appl. Mater. Interfaces*, 2019, **11**, 1267-1273.
17 Y. Yan, X. R. Shi, M. Miao, T. He, Z. H. Dong, K. Zhan, J. H. Yang, B. Zhao and B. Y. Xia, *Nano Res.*, 2018, **11**, 3537-3547.
18 C. Lin, Z. Gao, J. Yang, B. Liu and J. Jin, *J. Mater. Chem. A*, 2018, **6**, 6387-6392.
19 D. Y. Chung, S. W. Jun, G. Yoon, H. Kim, J. M. Yoo, K.-S. Lee, T. Kim, H. Shin, A. K. Sinha, S. G. Kwon, K. Kang, T. Hyeon and Y.-E. Sung, *J. Am. Chem. Soc.*, 2017, **139**, 6669-6674.
20 D. J. Li, J. Kang, H. J. Lee, D. S. Choi, S. H. Koo, B. Han and S. O. Kim, *Adv. Energy Mater.*, 2018, **8**, 1702806.
21 H. Lu, W. Fan, Y. Huang and T. Liu, *Nano Res.*, 2018, **11**, 1274-1284.
22 Z. Lai, A. Chaturvedi, Y. Wang, T. H. Tran, X. Liu, C. Tan, Z. Luo, B. Chen, Y. Huang, G.-H. Nam, Z. Zhang, Y. Chen, Z. Hu, B. Li, S. Xi, Q. Zhang, Y. Zong, L. Gu, C. Kloc, Y. Du and H. Zhang, *J. Am. Chem. Soc.*, 2018, **140**, 8563-8568.
23 J. Xiao, Z. Zhang, Y. Zhang, Q. Lv, F. Jing, K. Chi and S. Wang, *Nano Energy*, 2018, **51**, 223-230.
24 R. Wang, X.-Y. Dong, J. Du, J.-Y. Zhao and S.-Q. Zang, *Adv. Mater.*, 2018, **30**, 1703711.
25 L. Najafi, S. Bellani, R. Oropesa-Nuñez, A. Ansaldo, M. Prato, A. E. Del Rio Castillo and F. Bonaccorso, *Adv. Energy Mater.*, 2018, **8**, 1703212.
26 L. Jiao, Y.-X. Zhou and H.-L. Jiang, *Chem. Sci.*, 2016, **7**, 1690-1695.
27 G. Ou, P. Fan, X. Ke, Y. Xu, K. Huang, H. Wei, W. Yu, H. Zhang, M. Zhong, H. Wu and Y. Li, *Nano Res.*, 2018, **11**, 751-761.
28 Y. Yu, Z. Peng, M. Asif, H. Wang, W. Wang, Z. Wu, Z. Wang, X. Qiu, H. Tan and H. Liu, *ACS Sustainable Chem. Eng.*, 2018, **6**, 11587-11594.
29 X. Zhu, M. Liu, Y. Liu, R. Chen, Z. Nie, J. Li and S. Yao, *J. Mater. Chem. A*, 2016, **4**, 8974-8977.
30 K. Wang, X. She, S. Chen, H. Liu, D. Li, Y. Wang, H. Zhang, D. Yang and X. Yao, *J. Mater. Chem. A*, 2018, **6**, 5560-5565.
31 W. Zhao, X. Lu, M. Selvaraj, W. Wei, Z. Jiang, N. Ullah, J. Liu and J. Xie, *Nanoscale*, 2018, **10**, 9698-9706.
32 S. H. Yu and D. H. C. Chua, *ACS Appl. Mater. Interfaces*, 2018, **10**, 14777-14785.
33 X. Gan, R. Lv, X. Wang, Z. Zhang, K. Fujisawa, Y. Lei, Z.-H. Huang, M. Terrones and F. Kang, *Carbon*, 2018, **132**, 512-519.
34 C. Wu, Y. Yang, D. Dong, Y. Zhang and J. Li, *Small*, 2017, **13**, 1602873.
35 S. Piontek, C. Andronescu, A. Zaichenko, B. Konkena, K. junge Puring, B. Marler, H. Antoni, I. Sinev, M. Muhler, D.

Mollenhauer, B. Roldan Cuenya, W. Schuhmann and U.-P. Apfel, *ACS Catal.*, 2018, **8**, 987-996.
36 Y. Chen, G. Yu, W. Chen, Y. Liu, G.-D. Li, P. Zhu, Q. Tao, Q. Li, J. Liu, X. Shen, H. Li, X. Huang, D. Wang, T. Asefa and X. Zou, *J. Am. Chem. Soc.*, 2017, **139**, 12370-12373.
37 J. Qian, Z. Li, X. Guo, Y. Li, W. Peng, G. Zhang, F. Zhang and X. Fan, *Ind. Eng. Chem. Res.*, 2018, **57**, 483-489.
38 B. C. Patra, S. Khilari, R. N. Manna, S. Mondal, D. Pradhan, A. Pradhan and A. Bhaumik, *ACS Catal.*, 2017, **7**, 6120-6127.